Euro. Jnl of Applied Mathematics (2015), *vol.* 26, *pp.* 795–819. © Cambridge University Press 2015
doi:10.1017/S0956792514000448

Interference in a three-dimensional array of jets

P. E. WESTWOOD and F. T. SMITH

Department of Mathematics, UCL, Gower Street, London WC1E 6BT, UK
emails: paul.e.westwood@btinternet.com, f.smith@ucl.ac.uk

(*Received 2 April 2014; revised 15 December 2014; accepted 21 December 2014; first published online 28 January 2015*)

The theoretical investigation here of a three-dimensional array of jets of fluid (air guns) and their interference is motivated by applications to the food sorting industry especially. Three-dimensional motion without symmetry is addressed for arbitrary jet cross-sections and incident velocity profiles. Asymptotic analysis based on the comparatively long axial length scale of the configuration leads to a reduced longitudinal vortex system providing a slender flow model for the complete array response. Analytical and numerical studies, along with comparisons and asymptotic limits or checks, are presented for various cross-sectional shapes of nozzle and velocity inputs. The influences of swirl and of unsteady jets are examined. Substantial cross-flows are found to occur due to the interference. The flow solution is non-periodic in the cross-plane even if the nozzle array itself is periodic. The analysis shows that in general the bulk of the three-dimensional motion can be described simply in a cross-plane problem but the induced flow in the cross-plane is sensitively controlled by edge effects and incident conditions, a feature which applies to any of the array configurations examined. Interference readily alters the cross-flow direction and misdirects the jets. Design considerations centre on target positioning and jet swirling.

Key words: air guns; food sorting; asymptotic theory; analysis; jets

1 Introduction

The motivation for the current study which involves modelling, asymptotic analysis and allied numerical work arose from the food-sorting industry, and there are applications also to inkjet printing, sprinklers and air guns for example. It is our great pleasure to dedicate this article to John Ockendon, a tower of strength in the area of industrial mathematics.

In the relevant food-sorting configuration huge numbers of grains (rice, peas, seeds, etc.) or similar small bodies are let fall rapidly down an inclined chute as discussed in [1, 2] and then drop off the end of the chute under gravity. At that stage the multiple grains then form a free-falling sheet in effect but they are viewed individually by means of an inspection laser, any faulty grain is identified and almost immediately an air jet is fired from a multiple high-pressure ejector machine which is intended to knock that faulty grain out of the free-falling sheet. There are many jets in order to cover the space mapped out by the sheet and they fire over remarkably short time scales of 3–10 msecs. Typically a single row of ejectors comprises many narrow ducts (nozzles) of a few mms in cross-section each of which is separated from its immediate neighbour by a gap of a fraction of a mm, which is governed by the thickness of the ejector walls. The firing from

the ejector nozzles is performed independently in response to faulty items entering the target areas, the air jet speed may be 20–40 m/sec and the transient phases of start-up and shut-down persist for a small fraction of the firing time for each nozzle. Some of the values quoted here and below may be approximate. Collateral damage in the sense of nearby non-faulty grains being hit accidentally is a considerable problem here, hinging on the overall performance of the jets as they emerge from the array of nozzles and interact not only with the targeted grain and its neighbours but also with the other jets in the array. The focus is thus on an array of air jets issuing into otherwise quiescent or non-quiescent air. Among other aspects of concern are the misdirection of the issued jets occurring in practical cases (leading to a lessened impact on the target grain), the relatively high-flow rates, and the effects of varying the nozzle shapes and positions within an array. The shapes of most direct interest to industry are usually rectangular or circular due among other things to their relative ease of manufacture.

Three features therefore stand out. The first is that interference between multiple jets is a potentially vital factor here. In addition, the axial flow profile emerging from a typical nozzle is usually far from being of a fully developed form and indeed exhibits, near the nozzle walls, edge layers which are relatively thin although not extremely thin as noted in [3,4]. See also [5–10]. This aspect generates an interest in allowing for plug-type inputs but with significant edge layers being present, i.e. a smoothed plug flow input in effect at the beginning of the representative jet. The model adopted in this paper in fact allows for arbitrary inputs of positive axial motion. Finally, the flow from a nozzle often has at least some element of swirl in it, a factor which the modelling should also aim to accommodate at some stage. The ensuing edge effects as the interference takes place between the three-dimensional (3D) jets in an array are of much interest.

Multiple two-dimensional (2D) jets and their interference have been studied in [11] based on the approach of [12] for 2D wake interference; see also [13], on transient growth of billets, where approximate averaging methods are used as distinct from the present rational approach on spatial evolution, and the reviews in [14]. Westwood [11] finds close agreement between computational results and a small-distance analysis, especially for a single jet, and also addresses the development of an unsteady jet. The nozzle array and accompanying configuration of real concern in the industry however are 3D, and it is taken here that the modelling study has to be spatially 3D by virtue of not only that geometry but also the complicated 3D fluid flows within the jets and the interactions between them. Being fully 3D implies that substantially new problems are to be encountered and that 2D or axi-symmetric approaches, as used in most previous theories, become perhaps questionable and /or invalid. Much theoretical, analytical and numerical work, and little experimental work of course, has been done on the 2D jet but rather the opposite is true of the more realistic 3D case.

For a typical jet in the industrial setting the Reynolds number based on a representative nozzle diameter of about 2–5 mm and incident axial velocity of about 20–40 m/s is approximately $4 - 6 \times 10^3$. The development length of the jet in the axial direction is then of the order of Re multiplied by the nozzle diameter, giving approximately 5m say. This is for laminar flow which is considered primarily in the present analysis although the work also applies to the turbulent regime as we shall see. The axial length of concern to the industry on the other hand as regards impacts on target grains is about 150 mm,

https://doi.org/10.1017/S0956792514000448 Published online by Cambridge University Press

a distance that is large compared with the nozzle diameter but small compared with the development length of 5 m evaluated above. (The situation is thus very suitable for asymptotic treatment of course.) In consequence our interest is to be in axial behaviour over a long length scale but still short relative to the viscous scale. Moreover, a fairly general 3D configuration is accommodated in the present work, allowing for various arrays of variously shaped nozzles as well as various sizes of different input velocity from each nozzle in order to be able to model the effects of distributed and phased firing of the fluid jets and the possible influences of changes in nozzle design.

Given that the incident velocity profiles of most present concern are of under-developed type (having edge layers as described earlier), or are less smooth in a sense, and they are issuing from many nozzles, a direct computational approach is likely to have some difficulty in dealing well with the 3D case in full. In contrast the 3D case appears to yield well to an analytical asymptotic approach exploiting the slenderness of the jets, the long but not excessively long axial scales of interest and the limited but not extremely limited smoothness of the input. These properties enable the task to be reduced from a 3D to an effective 2D problem by accounting for the feedback and interaction between the cross-plane and axial responses in the jets. The edge effects in particular are found to be important in controlling the directions of the jets.

The present article describes a theoretical examination of incompressible 3D steady or unsteady flow within a 3D array of jets, then. Section 2 below describes the model system under discussion in which a relatively long axial length scale is supposed, from nozzle to target; the analysis leads through validated steps based on asymptotic analysis to a reduced 2D interactive problem for the 3D longitudinal vortex-like behaviour in the jet array. Any nozzle cross-section and any number of them can be accommodated in principle in the analysis. Analytical based solutions are addressed in Sections 3–6. These help in exploring the vast parameter space. Smooth and non-smooth inputs from the nozzle jets, multiple inputs from multiple nozzles, swirl effects and unsteadiness are considered, and cross-flows are especially examined in the results. The work includes proof of non-periodicity in the solution. Further comments are then presented in Section 7, including design implications.

2 The three-dimensional jets

The model configuration has an array of nozzles whose cross-sectional planes lie in or nearly in the same plane, of y, z, and from which jets of incompressible fluid issue in or approximately in the direction of x, where x, y, z are non-dimensional Cartesian coordinates as in Figure 1. The corresponding velocity components are u, v, w, respectively and the fluid pressure is p. The distance of interest in the axial direction x is that between representative nozzle and target and typically it is comparatively large, while the jets themselves evolve over an even longer axial distance. The non-dimensionalization used here is based on a representative nozzle diameter, on a typical incident axial velocity of a jet and on the fluid density, yielding a Reynolds number Re in the Navier–Stokes equations with laminar flow assumed. The present investigation is of reduced systems based on asymptotic properties to predict the flow produced by the array of fluid jets issuing into otherwise quiescent or non-quiescent identical fluid. The typical non-dimensional 3D

https://doi.org/10.1017/S0956792514000448 Published online by Cambridge University Press

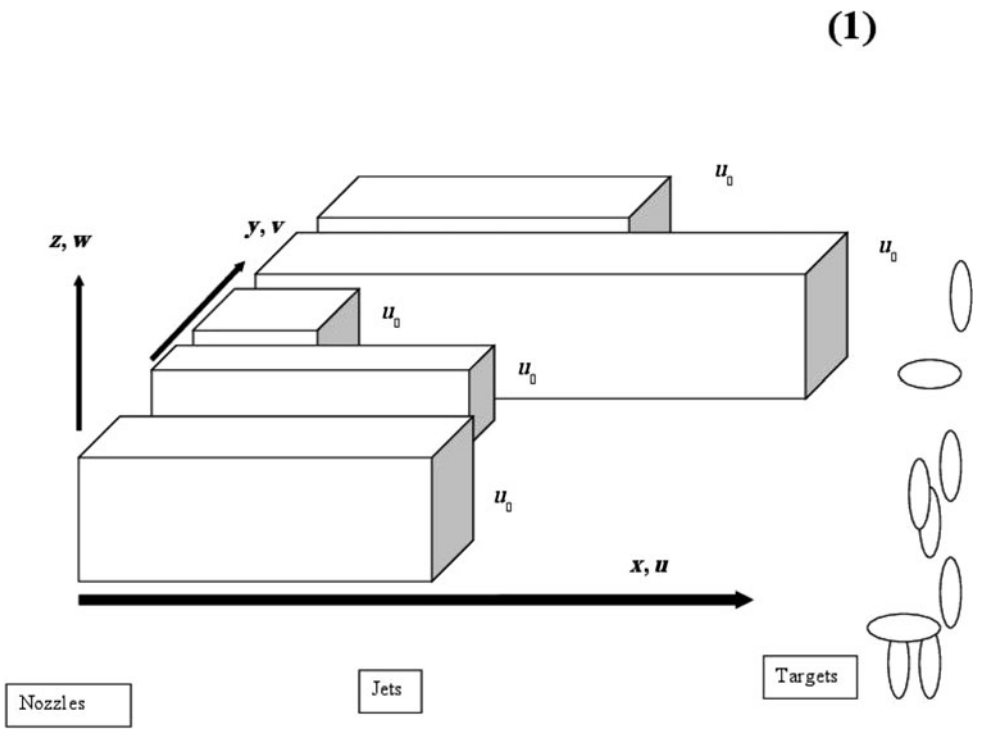

FIGURE 1. Sketch of the 3D jet array firing. Generally the input profile u_0 depends on y, z, t.

jet in the array is to be examined over an axial length scale L corresponding to the nozzle-to-target distance which is large whereas the cross-sectional length scales remain of $O(1)$ by definition, unless the cross-section of the jet and/or direction of the original nozzle at the inlet is particularly distorted.

For steady motion which is the starting point for this investigation (the comparison with unsteadiness is examined later in Section 6) the spatial scalings

$$x = LX, \quad y \sim z \sim 1, \tag{2.1}$$

apply with X of $O(1)$ and $1 \ll L \ll Re$ as explained earlier, and then the flow solution expands in the form

$$[u, v, w, \Omega] = \left[u_0 + \gamma\, u_1 + \cdots, Re^{-1}(v_0 + \gamma v_1 + \cdots), Re^{-1}(w_0 + \gamma w_1 + \cdots), Re^{-1}(\Omega_0 + \gamma\, \Omega_1 + \cdots)\right], \tag{2.2a}$$

$$p = \pi_1 + O(\gamma) + Re^{-2}(\pi_2 + O(\gamma)) + \cdots. \tag{2.2b}$$

The secondary vorticity $\Omega = W_y - V_z$ is introduced here for convenience. Also the parameter $\gamma = L/Re$ is small. The scalings on velocity are implied by the continuity balance while those involved in the pressure response stem from the axial momentum balance as far as the $O(1)$ term independent of y, z is concerned and from the cross-sectional momentum equations for the $O(L^{-2})$ contribution which depends on y, z as well

https://doi.org/10.1017/S0956792514000448 Published online by Cambridge University Press

as X. Two points stand out here, namely that the ratio γ of the target distance L over the Reynolds number Re is important since the latter yields an inertial–viscous balance of forces corresponding to the viscous development length scale, and that the leading order pressure π_1 and its $O(\gamma)$ correction must be constant in order to match to effectively zero axial flow outside the jet or jet array. The balances in the Navier–Stokes equations then point to the appropriate form of the solution being

$$[u_0, v_0, w_0, \Omega_0] = [U_0(y,z), V_0(y,z), W_0(y,z), -\zeta_0(y,z)]\,, \text{ with } \pi_1 = 0, \tag{2.3}$$

at leading order, where X dependence is absent thus far. One could of course argue that the Re^{-1} scalings in equation (2.2a) should be increased to L^{-1} in order to allow for the possibility of u_0 being dependent on X but subsequent reasoning is found to lead back to the self-consistent form of equations (2.2a) with (2.3). The pressure π_1 is set as zero without loss of generality. At next order the implied solution form is

$$[u_1, v_1, w_1, \Omega_1] = X\,[U_1(y,z), V_1(y,z), W_1(y,z), -\zeta_1(y,z)]\,, \text{with } \pi_2 = \pi_2(y,z), \tag{2.4}$$

and X, y, z dependence again is shown explicitly. Hence the continuity equation becomes

$$U_1 + V_{0y} + W_{0z} = 0, \tag{2.5a}$$

along with the X-momentum equation

$$U_0 U_1 + V_0 U_{0y} + W_0 U_{0z} = \Delta\, U_0, \tag{2.5b}$$

and the cross-sectional momentum balances

$$U_0 V_1 + V_0 V_{0y} + W_0 V_{0z} = -\partial\pi_2/\partial y + \Delta V_0, \tag{2.5c}$$

$$U_0 W_1 + V_0 W_{0y} + W_0 W_{0z} = -\partial\pi_2/\partial z + \Delta W_0. \tag{2.5d}$$

Here, Δ is the 2D Laplacian operator $(\partial_y{}^2 + \partial_z{}^2)$ since longitudinal diffusion is negligible over the current axial length scales.

The governing equations of concern then are the long-scale ones; equations (2.5a)–(2.5d). Once the incident flow with $u = U_0(y,z)$ say at $X = 0$ is appropriately defined, the system which is elliptic in the cross plane of y, z can be solved in principle to predict the flow velocities and pressures everywhere. The three-dimensionality of the motion makes the task of solving a relatively complex task, as does the need to deal with the multiple inlets especially as we would wish to accommodate many types of nozzle shape, see Figure 1, as well as provide some analytical and/or physical insight from which analysis concerning interference might develop. We shall incorporate in general a non-symmetrical array of nozzles and corresponding non-symmetrical 3D jet flow. Again, clearly the typical angles of divergence or convergence of the jets here are assumed small and of order $1/L$ from the length scales in equation (2.1) or $1/Re$ from the velocity scales in equation (2.2a). We recall that the length scale L above satisfies $1 \ll L \ll Re$. At one extreme, on the $O(Re)$ length scale in general viscous filling of the representative jet flow and of the flows in its neighbours takes place along with nonlinear inertial–viscous balancing as described

https://doi.org/10.1017/S0956792514000448 Published online by Cambridge University Press

in [15,16] together with incident boundary conditions at the upstream inlet positioned at $X = 0$ say and a condition of no axial flow, $u \to 0$, in the far field outside the jet array. (In the far field the cross-flow velocities V, W decay slowly in the 3D case, whereas 2D cases would yield $O(1)$ lateral velocities.) The paper [15] also shows good agreement with direct simulations of the Navier–Stokes equations at realistic Reynolds numbers. On the $O(1)$ length scale, at the other extreme, the full Euler equations would apply at leading order except that their solution is the uni-directional flow associated with U_0 in equation (2.3). Higher order contributions satisfy linear equations forced by the small viscous effects due to U_0 in essence.

It is preferable to work in terms of the vorticity and velocity, thus replacing equations (2.5a)–(2.5d) by

$$U_0\zeta_1 + V_0\zeta_{0y} + W_0\zeta_{0z} = \zeta_0(V_{0y} + W_{0z}) - U_{0z}V_1 + U_{0y}W_1 + \Delta\zeta_0, \tag{2.6a}$$

$$\Delta V_0 = \zeta_{0z} - U_{1y}, \tag{2.6b}$$

$$\Delta W_0 = -\zeta_{0y} - U_{1z}, \tag{2.6c}$$

$$U_0U_1 + V_0U_{0y} + W_0U_{0z} = \Delta U_0; \tag{2.6d}$$

the alternative equation $\zeta_0 = V_{0z} - W_{0y}$ can be used in place of equation (2.6c). Here it can be seen that U_0, ζ_0 must be regarded as known input (V_0, W_0 for instance cannot be specified arbitrarily). All other quantities in (2.2a)–(2.5d) are in effect unknowns in the jet motion and are governed by (2.6a)–(2.6d) with appropriate boundary conditions. The perhaps surprising feature that the precise cross-flow V_0, W_0 even at leading order is among the unknowns is in keeping with previous 2D findings [12]. Working with equations (2.6a)–(2.6d) is generally more useful here than with the counterparts derived in equations (2.5a)–(2.5d).

Another notable feature is that the 3D flow solution is non-periodic in the cross-plane even if the nozzle array itself is periodic. The feature applies for any input profiles and is demonstrated later in the article. Also, in terms of a check, marching computations for a 3D jet were made on the basis of a Cartesian gridding method as in [15,17], over the longer $O(Re)$ axial scale where 3D longitudinal-vortex equations hold. Agreement between the marching computational results at decreased lengths and the $O(L)$ based analysis in equations (2.1)–(2.5d) is found for a smooth u_0 profile as demonstrated in [11]; this is essentially for a single jet. The marching computational approach necessarily has a certain amount of difficulty with satisfactory handling of less smooth input profiles from many nozzles, which is the case of most present concern, a feature that helps to motivate the subsequent more analytical work.

3 Properties for smooth jets

Our eventual concern lies with less smooth inputs and with multiple jets as just stated. A central case seems desirable for this. To be specific we take as one central form here that of zero input swirl, meaning that ζ_0 is identically zero. ([11] examines some effects due to nonzero swirl for a single jet and we examine swirl effects for many jets in Section 6).

https://doi.org/10.1017/S0956792514000448 Published online by Cambridge University Press

Then equations (2.6b)–(2.6c) reduce to

$$\Delta V_0 = -U_{1y}, \tag{3.1a}$$

$$\Delta W_0 = -U_{1z}. \tag{3.1b}$$

So with U_1 also undetermined as yet equations (3.1a) and (3.1b) with (2.6d) provide three coupled equations for the induced axial correction U_1 and the leading-order cross-flow velocity components V_0, W_0. Working similar to that in this and the next two sections holds wherever the secondary vorticity is identically constant: see Section 6.

An example for a single jet in which

$$U_0 = 1/(1 + y^n + (z/H)^n) + c, \tag{3.2}$$

and the input swirl is zero is presented in Figure 2 for two distinct cases, a square and a rectangle. (The numerical work is based on iteration with standard central-differencing throughout.) Here n, c, H are positive constants and there is much interest in the effects of increasing the integer power n, thus making the input velocity profile increasingly less smooth. As n becomes larger the form in equation (3.2) tends to pick out the edges of the rectangle where $|y| = 1$, $|z| = H$ and U_0 tends towards a discontinuous profile; in Figure 2(a) and (b) H is $1/3$ to represent an approach to a thin rectangle whereas Figure 2(c) has H as unity for an emergent square. The influence on the cross-flow is a marked one, in line with the analysis in the next section. Figure 2 is with U_0 as in equation (3.2) and $c = 0.05, n = 10$. Local results from two different grids and/or outer boundaries agree reasonably well, confirming that v is odd in y, w is even in y, given the input symmetry, while the inward suction effect seen in the "far field" is as expected physically. Many different cases could be computed thus but we want to have many jets altogether.

Examples with two jets essentially of quite thin rectangular planform in which U_0 is similar to the type just mentioned are presented in Figure 3. In detail the figure has two smooth jets for two cases (a), (b) each with U_0 as in equation (3.2) with $c = 0.05, n = 10$ but displaced horizontally by a distance of 3 giving relatively thin nozzles side by side: (a) is for two emergent squares and (b) for two emergent rectangles. Here and below, results from a doubled grid agreed well with those shown. The symmetry about $y = -3/2$ is as expected. See also thin-body theory later. Given the above we may turn now to non-smooth input from multiple jets.

4 Analysis of plug-type jets

So far the working has assumed that the input axial profile $U_0(y, z)$ is smooth. For plug-type profiles we let U_0 approach a discontinuous form

$$U_0 = \text{ constant inside } C \text{ and constant outside } C, \tag{4.1a}$$

for the typical jet within an array, where C is the boundary edge of the jet. Here the constants are nonzero usually, while very close to and astride C a thin smoothing region or edge layer of thickness $\varepsilon(\ll 1)$ matches U_0 locally to the two constants on either side

https://doi.org/10.1017/S0956792514000448 Published online by Cambridge University Press

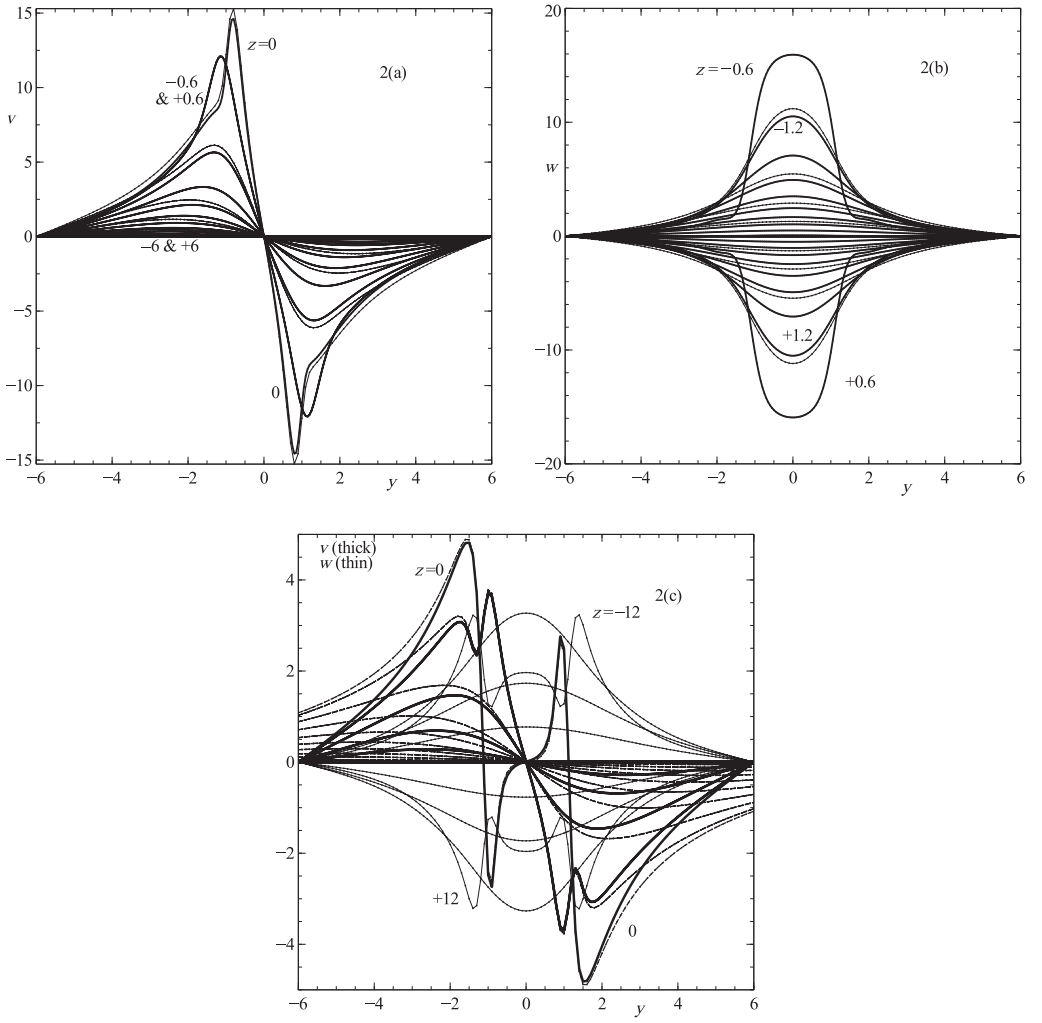

FIGURE 2. Results for a single smooth jet in two cases. Here U_0 is as in equation (3.2) with $c = 0.05, n = 10$. (a) and (b) Emergent rectangle measuring 1 (horizontal) by 1/3 (vertical). Plotted are v, w against y at fixed z stations. (c) Emergent rectangle 1 by 1, i.e. square.

of C, such that

$$U_0 = U_{00}(N) \text{ astride the edge } C \tag{4.1b}$$

where N is the scaled lateral coordinate within the edge layer and U_{00} is smooth in N. An exponential profile of U_{00} is usually kept in mind. The form in equation (4.1a) and (4.1b) is to be applied to the approach in equations (2.6d), (3.1a) and (3.1b). The alternative of specifying U_0 as discontinuous right from the start is worth just mentioning. It provokes $X^{1/2}$ edge layers (Chapman layers) at the edges, similar to those in the current scenario, but the present approach takes $\varepsilon \gg X^{1/2}$ from an order-of-magnitude argument which allows equations (4.1a) and (4.1b) to be used within the context of equations (2.6d), (3.1a) and (3.1b). The overall benefit of the present approach is that it accommodates a wide

https://doi.org/10.1017/S0956792514000448 Published online by Cambridge University Press

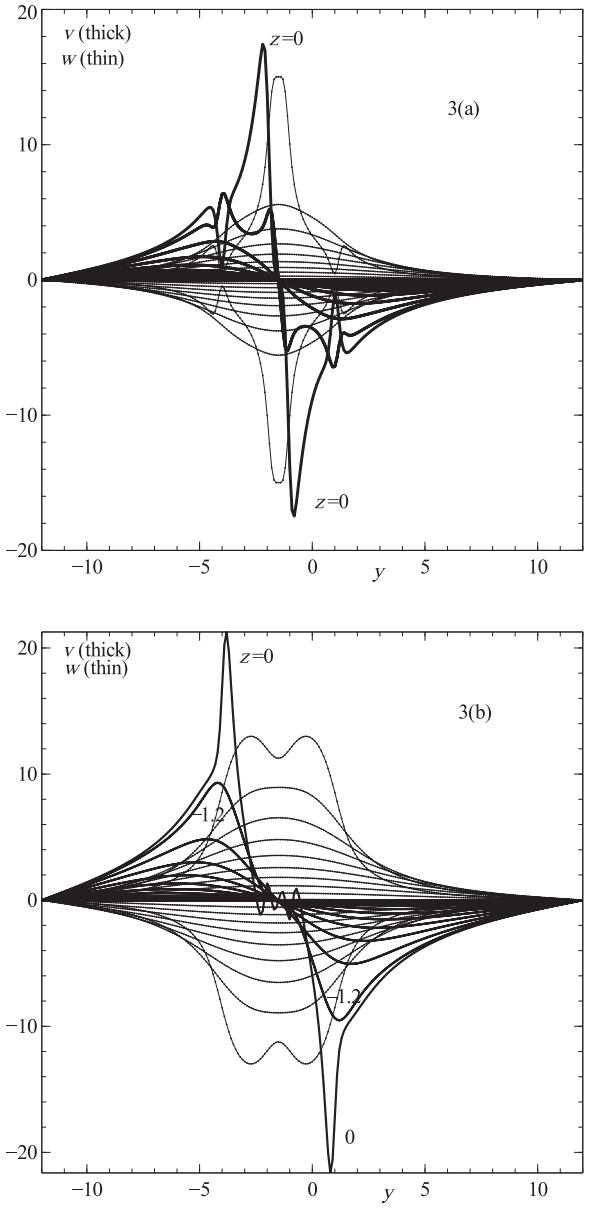

FIGURE 3. For two smooth jets. (a) Two emergent squares measuring 2 (horizontal) by 2 (vertical), occupying –4 to –2 and –1 to 1 in terms of y. Plotted are v, w against y at fixed z stations. (b) Two emergent rectangles 2 by 1/3, again with a gap of 3 between the centres of the jets.

range of input profiles. We mention also that the approach so far has taken U_0 as positive corresponding to forward axial motion but the following analysis also works with U_0 being zero outside C, or indeed inside C. The case of U_0 being zero outside the boundary or edge C will be treated subsequently as a limiting case.

https://doi.org/10.1017/S0956792514000448 Published online by Cambridge University Press

Given equation (4.1a), it follows from equation (2.6d) that $U_1 = 0$ throughout the bulk of the cross-plane. Hence the controlling equations there are the pair

$$\Delta V_0 = 0, \tag{4.2a}$$

$$\Delta W_0 = 0. \tag{4.2b}$$

The continuity equation with zero U_1 now reduces however to $V_{0y} + W_{0z} = 0$, while zero input swirl implies that $V_{0z} - W_{0y} = 0$, and so the scaled cross-flow stream function ψ and cross-flow velocity potential φ form a conjugate pair such that

$$V_0 = \varepsilon^{-1}\psi_z = \varepsilon^{-1}\varphi_y, \tag{4.3a}$$

$$W_0 = -\varepsilon^{-1}\psi_y = \varepsilon^{-1}\varphi_z. \tag{4.3b}$$

The factors ε^{-1} are explained below, and φ, ψ both satisfy Laplace′s equation,

$$\Delta\varphi = 0, \tag{4.4a}$$

$$\Delta\psi = 0. \tag{4.4b}$$

These apply in the majority of the cross-plane whereas the smoothing regions astride each edge C yield the jump requirement across each edge

$$\frac{1}{U_0{}^+}\left(\frac{\partial\phi^+}{\partial n}\right) - \frac{1}{U_0{}^-}\left(\frac{\partial\phi^-}{\partial n}\right) = -J, \tag{4.4c}$$

$$\text{where } J = \int_{-\infty}^{\infty}\left(\frac{U_{00}{}''}{U_{00}{}^2}\right)dN, \tag{4.4d}$$

on the velocity potential in particular. Here the superscripts $+, -$ refer to quantities on either side of the edge in the sense defined below and n is the un-scaled normal coordinate. The jump J is produced by the quasi-planar behaviour within the thin edge layer holding in terms of $N(= n/\varepsilon)$, such that if N is aligned with the y direction for instance then in effect equations (3.1a) and (2.6d) reduce respectively to

$$V_{0yy} = -U_{1y}, \tag{4.5a}$$

$$U_{00}U_1 + V_0U_{00}{}' = U_{00}{}'' \tag{4.5b}$$

to leading order, because of an expansion based on (4.1b), with z derivatives and allied effects being negligible; the solution of (4.5a) and (4.5b) for V_0 then gives J as above from matching at large N. Similar working applies for N lying in any direction, thus confirming equations (4.4c) and (4.4d). The factors ε^{-1} in the definitions in equations (4.3a) and (4.3b) and hence the $O(1)$ scaling on the jump contribution J stem from the scaling on N and indicate that the induced cross-plane velocities are in general relatively large for the less smooth input jet profiles here. We should remark that from an integration by parts the jump J is positive and that in principle it can depend on the distance s around the edge C although here J will usually be taken not to vary around

https://doi.org/10.1017/S0956792514000448 Published online by Cambridge University Press

a given edge. The effect J is a Coanda-like one. The physical balance of 3D effects, between the cross-plane dynamics in equations (4.2a), (4.2b)–(4.4a) and (4.4b) and the axial dynamics implicit in equations (4.4c) and (4.4d), is also noteworthy with the present reduction to an effectively 2D problem. The signs are such that a fluid particle leaving the jet has a relative velocity v/u less than that of a particle entering at the same location in X, s, i.e. there is net relative entrainment, as expected physically for a jet.

Although the normal derivative is discontinuous across the edge C as shown in equation (4.4c) the scaled potential function φ itself is continuous everywhere; it is also smooth everywhere except at C and without loss of generality φ can be set to zero at some internal point inside C for example. Adding a constant to φ does not affect the induced velocities. Comparisons made in [11] between results from the reduced form in equations (4.4a)–(4.4d) and results for smooth velocity profiles as in Figures 2 and 3 which become increasingly less smooth tend to support the formulation in equations (4.4a)–(4.4d). Here the jump condition (4.4c) makes it perhaps most convenient to work with φ, while the boundary condition in the far field which is usually one of slow growth, $\varphi \sim -n_1 lnr + n_2$ where n_1, n_2 are $O(1)$ constants in general and r is the radial distance, can be accommodated in numerical cases by means of a three-point relation. This far-field response confirms that the cross-flow velocities decay slowly such that

$$\varepsilon(V_0, W_0) \sim -n_1(y, z)/r^2 \text{ in the far field,} \tag{4.6}$$

in most settings. By way of contrast, in a 2D case essentially, equation (4.4a) gives $d^2\varphi/dy^2 = 0$, leading to φ being linear in y which forces V_0 to be constant. In either scenario a source-like effect is induced in the far field.

The analysis for plug-type input is valid not only for all nozzle shapes but also for any number of nozzles as in an array. Linear superposition however does not apply generally because the required jump condition across the edge C of any jet in the array is affected by the solutions for all the other individual jets in view of the smoothness of their solutions at C. The factors $U_0{}^{\pm}$ in equation (4.4c) play an important role in this. On the other hand, if those factors are equal then superposition is seen to hold true, which enables analysis or computation for a wide variety of arrays to proceed. See [11] and techniques of potential flow and complex variables [18–20]. These issues are taken up in the following section.

5 Properties for plug-type jets

For the present plug-type jets or arrays (currently without swirl, we recall, but swirl is to be incorporated in the next section) the significance of the role of the edge velocity constants $U_0{}^{\pm}$ becomes clear mostly through examples within three categories as follows. These also lend themselves to examination of the solution behaviour when many jets are present.

5.1 Jets of different strengths

First if the edge velocities $U_0{}^{\pm}$ are unequal, which is the general case, then given there are clearly many possible parameters and jet nozzle shapes which could be considered here

https://doi.org/10.1017/S0956792514000448 Published online by Cambridge University Press

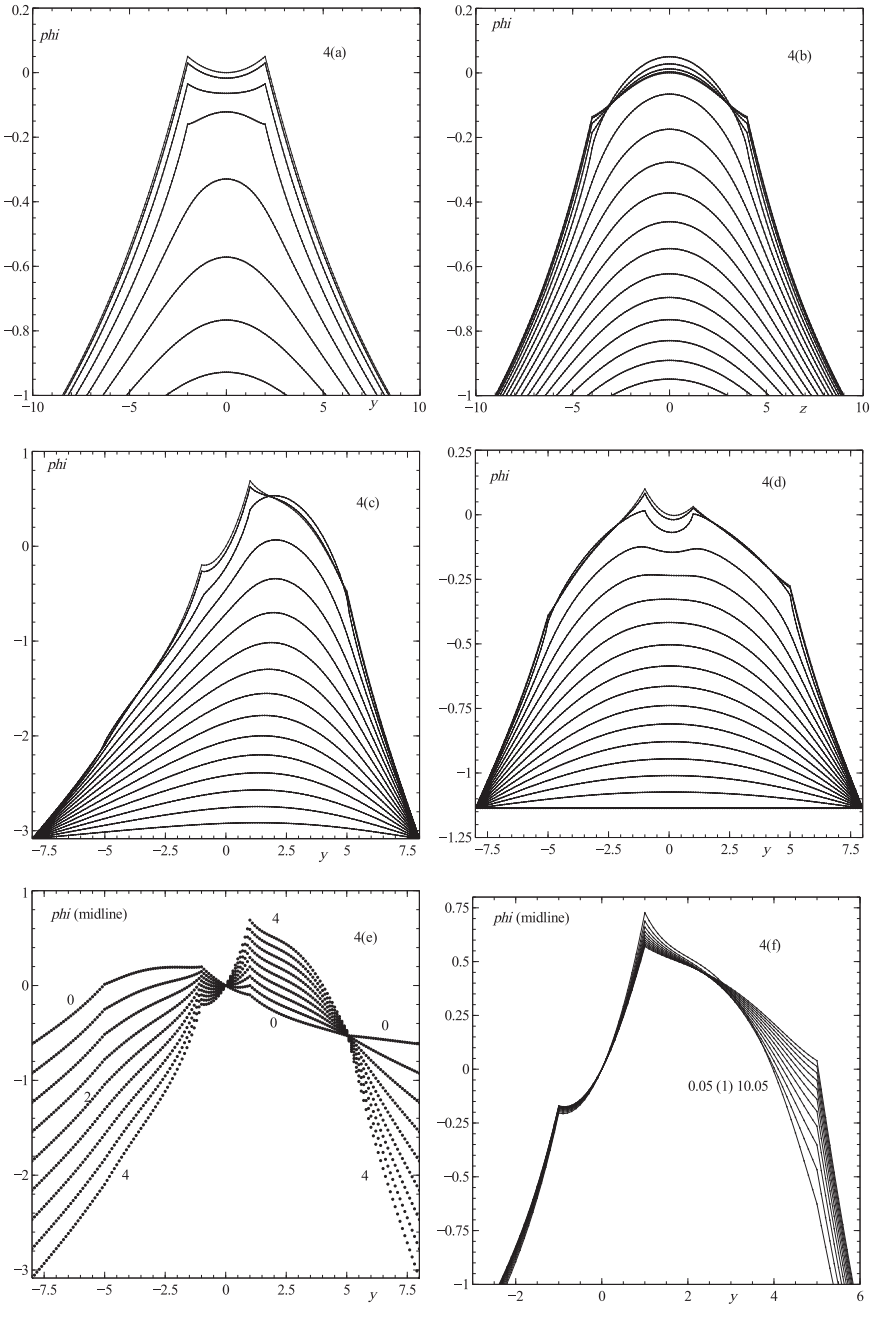

FIGURE 4. For plug cases with one or two rectangles, showing φ against y or z. (a), (b) One rectangle: φ versus y, z respectively. Here $(U_0{}^+, U_0{}^-) = (1, 0.25)$ and the edge jump $J = 1$. (c-i) Two rectangles each 4 by 2 (except in the final case (i)), under various conditions: (c) has $(U_0{}^+, U_0{}^{++}, U_0{}^-, J, J^+) = (1, 1, 0.25, 1, 4)$; (d) has $(0.5, 0.125, 0.25, 1, 1)$; (e) has $(1, 1, 0.25, 1, J^+$ varying), plotting φ at the midline $z = 0$; (f) has $(1, U_0{}^{++}$ varying, $0.25, 1, 4)$ where $1/U_0{}^{++}$ values are $0.05, 1.05, 2.05, \ldots, 10.05$; (g) has $(1, 1, U_0{}^-$ varying, $1, 4)$ with $1/U_0{}^-$ values $0.5, 1, 1.5, \ldots, 4$; (h) has $(1, 1, 0.25, 1, 4)$ but the gap width $G = 1(0.2)4$ varies from its usual value of 2; (i) has $(1, 1, 0.25, 1, 4)$ but the nozzle is a 4 by H rectangle with H values of 1(0.2)6.

https://doi.org/10.1017/S0956792514000448 Published online by Cambridge University Press

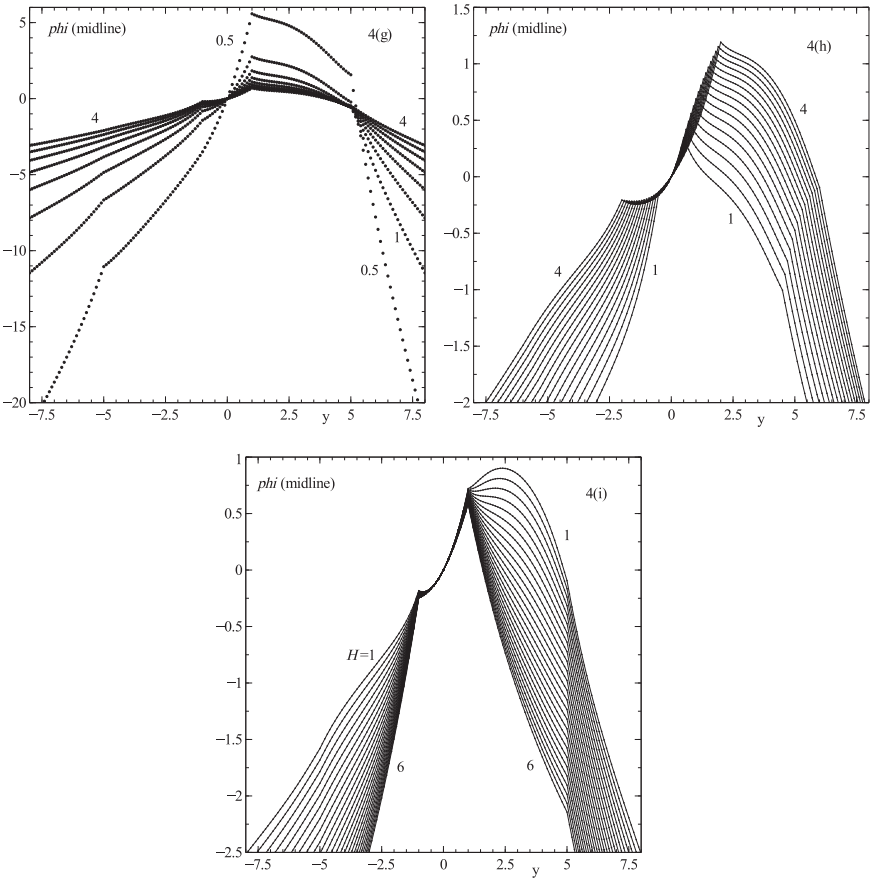

FIGURE 4. Continued

we highlight some major features through specific examples. Figure 4 gives the solution for φ when there are one or two rectangular nozzles: $(a),(b)$ are for a single rectangle and $(c)-(i)$ for two under various conditions. We remark as a reminder that the vertical velocity W_0 is essentially $\partial\varphi/\partial z$ and the horizontal V_0 is $\partial\varphi/\partial y$. The results indicate the effects of varying the edge velocities and also of introducing a neighbouring rectangular nozzle. Figure 4(a)–(i) indicates especially in (c) that on occasion the jumps at the outer edges of the rectangles can only just be seen whereas the inner jumps are clear. Also the J effects yield significant non-symmetry or skew and hence imply misdirection. The graphs here resemble the catenaries found later on. In (d) the skew is found to be the other way round compared with (c). Then (e) shows a variety of skew effects and specifically a marked switch-round within the gap in the middle, while (f) indicates only quite small skew effects being produced. Case (g) again shows considerably more variation in skew effects being produced. In (h) all examples have similar trends although the magnitudes increase with gap width, and similarly in (i) all cases have very similar results in the gap but wider variation inside the rectangles and beyond.

https://doi.org/10.1017/S0956792514000448 Published online by Cambridge University Press

Figure 5 gives the solution with one or more modelled rectangles side by side with aspect ratio of $O(1)$ arranged in a single row. The background requires some explanation. The simple model here is for zero φ or $\partial\varphi/\partial z$ on the upper and lower boundaries and allows an exact solution for any number (N) of jets. In the former case, we take $\varphi = \varphi_n(y)\sin(\Gamma z)$ in the typical nth nozzle where $H = \pi/\Gamma$ is the uniform nozzle height; the other case would have $\cos(\Gamma z)$ and yield the same working as below. Thus $W_0 \propto \varphi_n$ and $V_0 \propto \partial\varphi/\partial y$. In the figure, the strong influence of the edge velocity effects J in determining the momentum contributions within the array is evident. The equations involved begin with

$$\varphi_n = R_n \cosh(\Gamma(y - y_n)) + S_n \sinh(\Gamma(y - y_n)) \text{ in } n\text{th nozzle (for } n = 2 \text{ to } N - 1), \quad (5.1a)$$

in view of equation (4.4a). Here the array has nozzles and jets extending from $n = 1$ to $n = N$ with the respective axial edge velocity components being U_n, which are constants, and the jumps J being $j_n \sin(\gamma z)$ in turn where the j_n are given constants. The constants R_n, S_n are unknowns. The component equation (5.1a) holds for all but the endmost nozzles whereas the leftmost and rightmost ones have

$$\varphi_1 = A\exp(\Gamma y),\ \varphi_N = B\exp(-\Gamma y), \quad (5.1b)$$

respectively in line with decay in the far field, with the constants A, B to be found. The decay is exponential here rather than the algebraic form near equation (4.6) due to the continued constant height H in this example. Next, the junction requirements in equations (4.4c) and (4.4d) applied at each edge $y = y_n$ say yield two relations

$$R_{n+1} = R_n\tilde{c} + S_n\tilde{s}, \quad (5.1c)$$

$$S_{n+1}/U_{n+1} - (R_n\tilde{s} + S_n\tilde{c})/U_n = j_n/\Gamma, \quad (5.1d)$$

where $\tilde{c} = \cosh(\Gamma(y_{n+1} - y_n)), \tilde{s} = \sinh(\Gamma(y_{n+1} - y_n))$ and the edges may be uniformly spaced or not. An iterative scheme may then be set up to solve for all the component terms R_n, S_n such that the required end behaviours in equation (5.1b) are obtained and this produces catenaries as displayed in Figure 5. This figure presenting the modelled plug results covers several cases (i)–(vi) with varying jet velocities, locations, aspect ratios and edge jumps, all displaying suction flow at infinity again. Sample (iv) shows a strengthened effect due to the increased jumps j_n on the right in the diagram, whereas (v) and (vi) demonstrate that increased height H leads to more unevenness in V_0. Overall the results are in line with those in Figure 4 given earlier.

The main points to draw from the work include the ellipticity of the system and the huge variety of configurations available. Certain extremes of the edge velocity ratios are also of interest, while for Γ large or small we obtain the helpful cases of comparatively thin or thick nozzles which are addressed in other results such as in thin-shape theory below and clearly hinge on the factors Γy in equations (5.1a)–(5.1d). Also a configuration with many jets leads to an essentially continuum limit in which equations (5.1c) and (5.1d) tend to

$$R'\tilde{\tilde{c}} + S'\tilde{\tilde{s}} = 0, \quad (5.1e)$$

$$(R/U)'\tilde{\tilde{s}} + (S/U)'\tilde{\tilde{c}} = j/\Gamma, \quad (5.1f)$$

https://doi.org/10.1017/S0956792514000448 Published online by Cambridge University Press

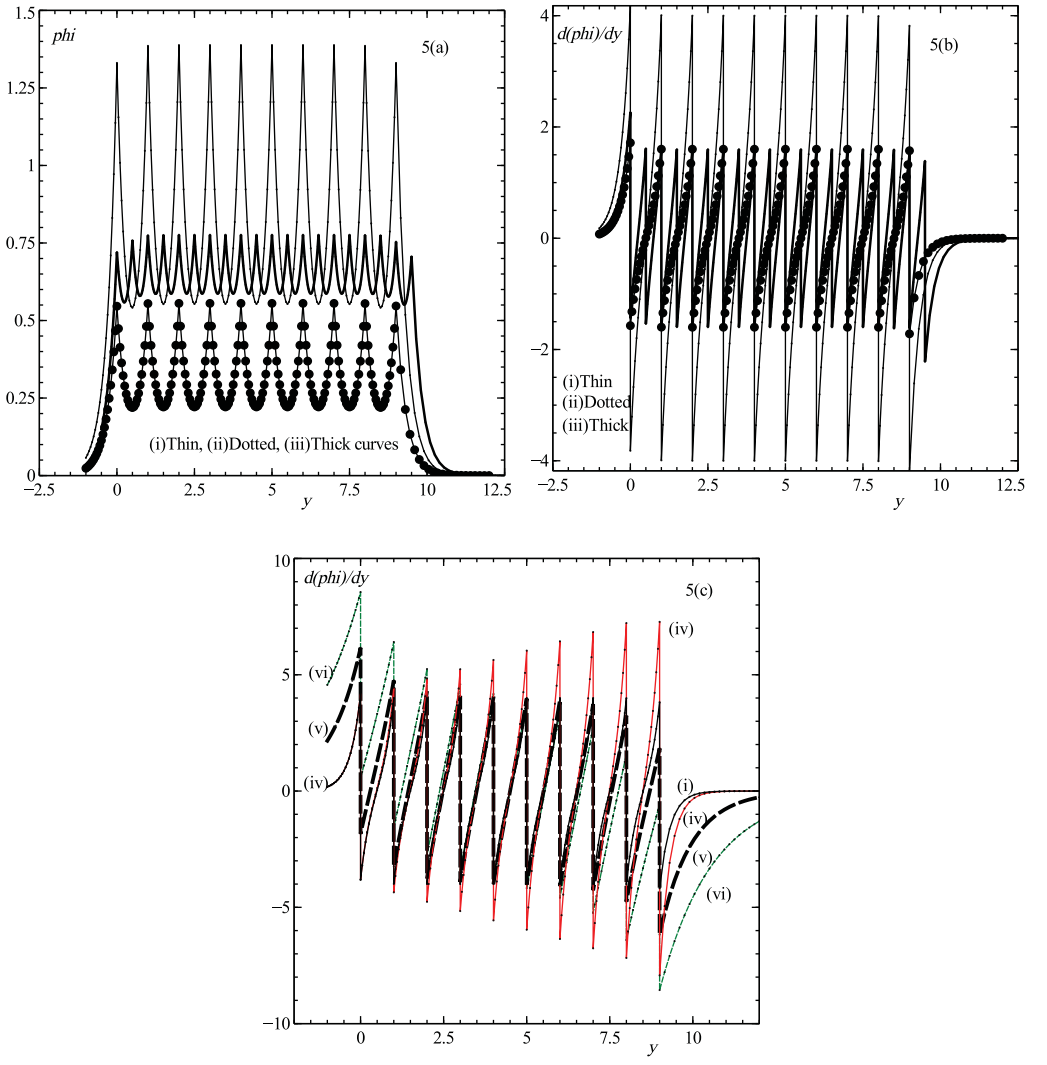

FIGURE 5. For modelled plug problem: (a)–(c) φ and $d\varphi/dy$ versus y for $(i)N = 11$, height $H = 1, U_n = 4(n \geqslant 2), j_n = 2$ centred on locations $y_n = n - 2$, (ii) is as for (i) but U_n are altered to 4 for odd n and 1 for even n, (iii) is as in (ii) except that $N = 21, y_n = (n-2)/2$; (c) $d\varphi/dy$ versus y for (iv), (v), (vi) along with original (i) for comparison. Here (iv) is for a different jump distribution while (v), (vi) have heights increased to 3, 5 respectively.

with $\Gamma\,\delta$ being of order unity where δ is the gap width and $R, S, U, j, \tilde{\tilde{c}}, \tilde{\tilde{s}}$ are respectively the continuous analogues related to the $R_n, S_n, U_n, j_n, \tilde{c}, \tilde{s}$ above. If U is constant throughout corresponding to equal edge velocities then (R', S') are given simply by $jU(-\tilde{\tilde{s}}, \tilde{\tilde{c}})/\Gamma$ whereas if U is not constant then from manipulation of (5.1e, 5.1f) the function R or S is governed by a non-simple second-order differential equation subject to endmost boundary conditions which are analogous to those of equation (5.1b) in the discrete case. The predicted value for $R(y)$ is reasonably close to the values seen in Figure 5 for an appropriate example. Overall these results are in keeping with the properties holding in

https://doi.org/10.1017/S0956792514000448 Published online by Cambridge University Press

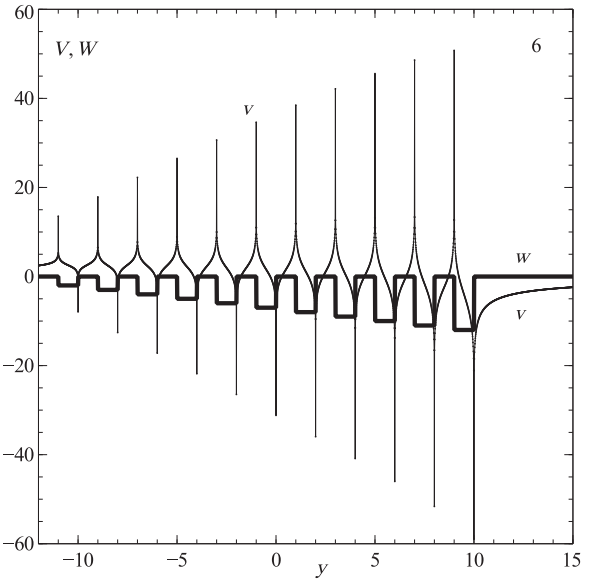

FIGURE 6. For thin rectangles: V, W versus y, along horizontal axis just above each rectangle.

the other two categories below, in particular they indicate the invalidity of superposition in the most common case of unequal edge velocities, they demonstrate again the ellipticity of the jet array problem, and they show non-periodicity of the flow solutions in general. The analysis can be extended from one to more rows in the vertical if necessary.

5.2 Equally strong jets

Next is the second category which has the constant values $U_0{}^{\pm}$ on either side of any jet edge being equal. This situation makes physical sense in terms of equally strong jets emerging from neighbouring nozzles and so being separated by a thin layer with zero axial velocity jump across that layer but inducing the normal velocity jump of equations (4.4c) and (4.4d). The study by [11] is within the current category. Highlighting is again called for in view of the many different configurations available in principle. Figures 612, 613, 619, 620 of [11] show solutions for 1 or 2 rectangles computed directly; the trends of the results agree with the more analytical work here.

Our Figure 6 on the other hand concerns any number of nozzles and focusses on thin rectangles or other thin shapes laid sequentially in end-on fashion, i.e. horizontally laid. Here thin-shape theory applies in terms of the small aspect ratio h say and can admit superposition of solutions in many cases. The relevant expansions are

$$\varphi = \bar{\varphi}_0 + h\bar{\varphi}_1 + h^2\bar{\varphi}_2 + \cdots \text{ inside any jet,} \tag{5.2a}$$

with $z = h\bar{z}$ and $\bar{z}$ of $O(1)$, so that $\bar{\varphi}_{0\bar{z}\bar{z}} = \bar{\varphi}_{1\bar{z}\bar{z}} = 0, \bar{\varphi}_{2\bar{z}\bar{z}} = -\bar{\phi}_{0yy}$, where φ is taken to be an even function. Therefore

$$\bar{\varphi}_0 = \bar{B}_0(y), \bar{\varphi}_1 = \bar{B}_1(y), \bar{\varphi}_2 = \bar{B}_2(y) - \frac{1}{2}\bar{B}_0{}''(y)\bar{z}^2. \tag{5.2b}$$

https://doi.org/10.1017/S0956792514000448 Published online by Cambridge University Press

Here $\bar{B}_0$ is an unknown function of y in particular. Outside the jets we have

$$\varphi = \varphi_0 + \cdots \tag{5.2c}$$

but with y, z of order unity, implying that Laplace′s equation controls φ_0 and so on. The boundary conditions are now of interest and indicate that φ_0 is the dominant function here. From equation (4.4c) at leading order φ_0 satisfies $\partial\varphi_0/\partial z = -JU_0^-$ at the jet edge together with equation (4.6) in the far field, conditions which are sufficient usually to determine ϕ_0 everywhere outside and give φ_0 on the jet edge. This also sets the edge value of $\bar{\varphi}_0$, in other words $\bar{B}_0$, for the calculation inside the jet, which can then go on to provide a slight correction to the outer problem by virtue of equation (5.2b), and so on. Hence a hierarchy is formed. If J is uniform say it follows specifically that the velocities produced just outside the jets are given by

$$\pi(V, W) = \Sigma K_n\{ln(r_1/r_2), \theta_2 - \theta_1\}, \tag{5.2d}$$

for an array of jets as presented in the above Figure 6. The figure is for thin end-on rectangles, where we find wide-ranging positive and negative values of velocity being produced and hence much implied misdirection. The quantities $K_n, r_1, r_2, \theta_1, \theta_2$ are the effective jumps, distances $|\mathbf{r} - \mathbf{r}_{1n}|$ and $|\mathbf{r} - \mathbf{r}_{2n}|$ from a typical field point $\mathbf{r}$ to each nozzle end, and the corresponding field-point angles, in turn, while the summation is over the rectangles or other thin nozzles in operation. Superposition applies at leading order in this category. The pattern of the solution agrees with the results in [11]. It is noted in passing that an interesting modification occurs if the thin-shape theory of equations (5.2a)–(5.2d) is combined with the extreme-ratio theory of the next paragraph to yield an integral equation for the unknown function $\bar{B}_0$ since, in general, a Cauchy–Hilbert integral describes the solution of equations (4.4a) and (4.4b). The thin-shape working in fact holds in modified form for all of the three categories addressed in the present section. We refer also to the analysis described in the previous paragraph.

5.3 Relatively strong jets

Thirdly, there is the category corresponding to relatively strong jets or to a plug jet or jets surrounded by almost quiescent fluid. Here one of the edge velocity constants is much larger than the other, $U_0^+ \gg U_0^-$ or vice versa. The highlights are the following. The analytical theory for this category rests on the relative increase in the velocity influence due to the $1/U_0^-$ factor in equation (4.4c). The prime formulae involved in the analysis turn out to be:

$$\partial\varphi^-/\partial n = -JU_0^- \text{ on } C, \tag{5.3a}$$

for the outside flow say, which satisfies Laplace′s equation and so acts to determine the function $\varphi^-(= \Phi$ say) on the jet edge C; and

$$\varphi^+ = \Phi \text{ on } C \tag{5.3b}$$

for the inside flow from (4.4c). Then Laplace′s equation for φ^+ with equation (5.3b) gives us φ^+ everywhere inside, hence $\partial\varphi^+/\partial n$ on C and hence a small correction to equation

https://doi.org/10.1017/S0956792514000448 Published online by Cambridge University Press

(5.3a) and so on, leaving us with a suction effect first (outside say) as in equation (5.3a) and then an internal adjustment (inside). This third-category framework but with the suction effect acting inside a jet area enclosed by C is similar to that for suction acting outside except for the mean influence which can be treated separately as for the circular case where φ is zero within C and $-\bar{J}ln(r)$ outside to within an additive constant, for any edge velocity ratio and effective jump $\bar{J}$. The asymptotic form shows the hierarchy above which in turn re-confirms the role of the edge velocity constants. The structure is similar to the second part of the second category in equations (5.2a)–(5.2d) although here there is no restriction on the shape of the nozzles involved in the interaction.

For the specific example of one or more circular nozzles the induced velocities take the form

$$\pi(V_m, W_m) = \Sigma A_n\{y - y_n, z - z_n\}/(\mathbf{r} - \mathbf{r}_n)^2, \tag{5.4}$$

where the array summation is over the circular nozzles in operation with n not equal to m and the A_n are the effective jumps for each nozzle. If many jets are operating then the overall elliptic effect and slow decay with distance are apparent, for instance along $z = z_n = 0$ where an alternating series gives V_m. Results are presented in the next section in order to compare them against the associated ones with swirl included. For the example of thin vertically laid rectangles on the other hand the analysis yields instead

$$\pi V_m = -2\Sigma B_n\theta_{1n}, \tag{5.5}$$

in contrast with the horizontally laid arrangement of equations (5.2a)–(5.2d). The summation now is over all n and the multiplicative factor for the jump effects B_n is halved at zero n, with equation (5.5) applying along $z = 0$ where W is zero, with θ_{1n} denoting $\arctan(\frac{1}{2}H_n/(y - s_n))$ and with the relative gap widths $H_n/[s_n - s_{n-1}]$ held uniform. Superposition only applies for such an infinitely long array by virtue of symmetry. Figure 7 displays the results for a number of these vertically laid rectangles. The figure actually concerns any thin broadside-on bodies uniformly spaced in a large (long) array. Results for small values of the gap width G point to the simple straight-line solution, in contrast with the boundary-layer-like response for large G values. The height H is kept fixed at unity.

6 Effects of swirl and unsteadiness

Properties for general swirl distributions are perhaps best approached via specific cases again and in that spirit the current section will consider briefly effects from constant swirl, followed by study of the unsteady regime. Before then however a proof of non-periodicity for the general case is given.

6.1 Non-periodicity in the general case

This concerns the solution for the cross-plane velocities with or without input swirl ζ_0. Returning to the original form in equations (2.5a)–(2.5d) for general input profiles we

https://doi.org/10.1017/S0956792514000448 Published online by Cambridge University Press

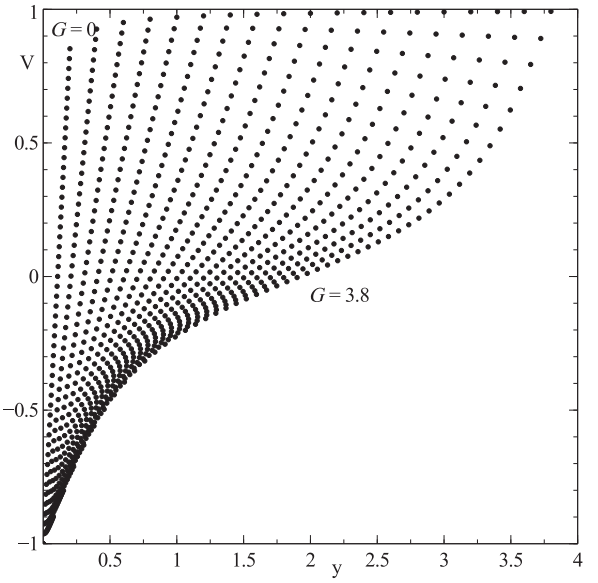

FIGURE 7. For thin bodies broadside-on in a large (long) array: V versus y along $z = 0$ in a representative gap for various scaled gap widths G.

eliminate U_1 between equations (2.5a) and (2.5b) to obtain the relationship

$$(V_0/U_0)_y + (W_0/U_0)_z = -\Delta(U_0)/{U_0}^2, \tag{6.1}$$

between the cross-plane velocity components V_0, W_0, in which the axial velocity U_0 is assumed known as stated earlier. The situation of interest here has the input $U_0(y, z)$ being periodic in the cross-plane coordinates y, z, say with periods M_y, M_z respectively. Supposing V_0, W_0 to be periodic over those periods then leads to a contradiction since the double integral of equation (6.1) with respect to y, z over the periods gives zero on the left-hand side but a nonzero contribution on the right-hand side. The latter contribution is

$$-2 \int \int_{(over M_y, M_z)} \left[({U_0}_y{}^2 + {U_0}_z{}^2)/{U_0}^3 \right] dy\, dz, \tag{6.2}$$

after an integration by parts, and clearly this contribution is nonzero and negative in general since U_0 is positive in general. The contradiction between the two sides establishes that V_0, W_0 cannot be periodic.

The main inference, that even if there is periodicity in the input axial velocity, in the input swirl and implicitly in the nozzle array the resulting flow in the cross-plane cannot be periodic, supports the view of some alteration in the direction of the input jet motion having to take place. In other words misdirection is inevitable. The question of how much misdirection occurs is answered largely by the specific results throughout Sections 2–6.

https://doi.org/10.1017/S0956792514000448 Published online by Cambridge University Press

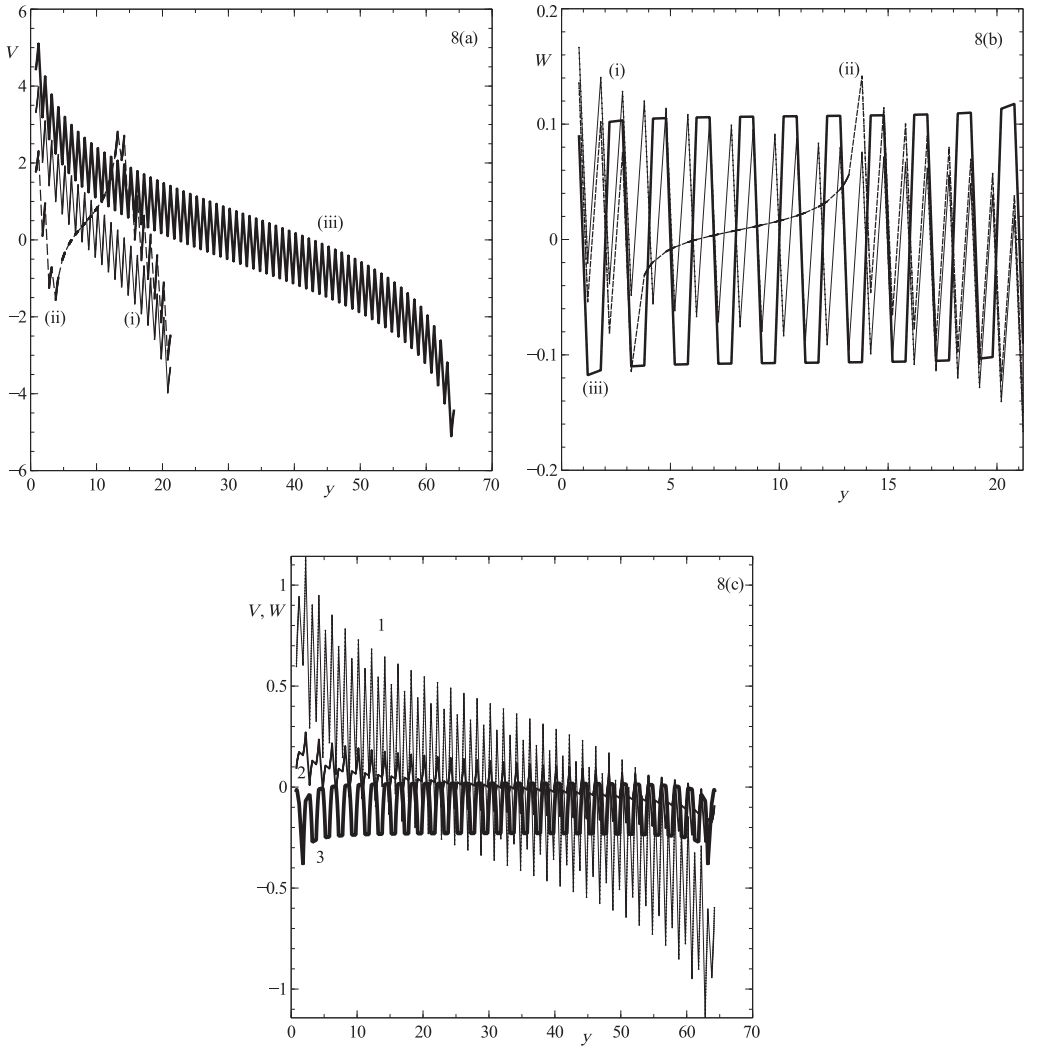

FIGURE 8. For circles with or without swirl. (a) No swirl: (*i*) 21 equispaced circles, all firing, with $A_n = -1$; (ii) as (i) but nos 4–13 switched off; (iii) 64 all firing. (b) With swirl dominating, this shows W versus y for: (*i*) total $N = 21, \kappa_n = 1$ for all n, radii= 0.2; (ii) as (i) but switched off nos 4-13; (iii) all 'on' but $\kappa_n = (-1)^{(n+1)}$. (c) For a double bank of nozzles, each bank having A_n constant and $\kappa_n = (-1)^{(n+1)}$, plotting V, W against y along the axis of the lower bank. The "1", "3" are V, W for $A_n = 0.1$ while "2" is V for $A_n = 0.02$.

6.2 Nonzero uniform swirl

Virtually the same working as in Sections 3 and 4 is found to apply wherever the secondary vorticity ζ_0 is identically K, a constant: then equations (3.1a) and (3.1b) still hold true but the relation $V_{0z} - W_{0y} = K$ must be satisfied also. If the input secondary swirl ζ_0 is piecewise constant then equations (3.1a) and (3.1b) remain valid inside each C, while if the input axial velocity U_0 is also piecewise constant then U_1 is zero, which yields equations

https://doi.org/10.1017/S0956792514000448 Published online by Cambridge University Press

(4.2a) and (4.2b). Coupled with this $V_{0z} - W_{0y} = K$ where K is the swirl constant within C. Hence now the quasi-potential is defined conveniently by

$$V_0 = \varepsilon^{-1}(\varphi_y + \kappa z/2), \tag{6.3a}$$

$$W_0 = \varepsilon^{-1}(\varphi_z - \kappa y/2), \tag{6.3b}$$

inside each C, given that K must be $O(\varepsilon^{-1})$, say $\varepsilon^{-1}\kappa$, to influence the dominant behaviour. It follows that equation (4.4a) still applies for φ. As regards the jump conditions across the edge C where more locally smoothing takes place between the different constant values of U_0, K the balances in equations (4.5a) and (4.5b) remain dominant astride C and so there V_0 is as before. Stemming from that, the jump requirement in equation (4.4c) still applies except that on the left-hand side $\partial\varphi/\partial n$ has to be replaced by $\partial\varphi/\partial n - \kappa r\cos(\theta - \alpha)/2$ in each occurrence due to equations (6.3a) and (6.3b). Here r, θ are polar coordinates inside C such that $(y, z) = r(\cos\theta, \sin\theta)$ and $\tan\alpha$ is the slope of the edge at the point (y, z) on C. The inference is that the jump requirement becomes

$$(\partial\varphi^+/\partial n)/U_0{}^+ - (\partial\varphi^-/\partial n)/U_0{}^- = -J^*, \tag{6.4a}$$

$$\text{where } J^* = J + \frac{1}{2}\left[\{\kappa r\cos(\theta - \alpha)/U_0\}^+ - \{\kappa r\cos(\theta - \alpha)/U_0\}^-\right], \tag{6.4b}$$

with the superscripts again denoting properties on either side of the typical edge C. The influence of the piecewise constant swirl here is to replace J by J^*, i.e. to alter the jump function in any particular case, and accordingly the earlier approach with zero swirl would seem to go through. There is a second influence however, which is on the continuity of φ effectively; it arises from the required continuity of the tangential velocity component at C to leading order and it imposes the jump condition

$$\partial\varphi^+/\partial s - \partial\varphi^-/\partial s = -\frac{1}{2}[\{\kappa r\sin(\theta - \alpha)\}^+ - \{\kappa r\sin(\theta - \alpha)\}^-], \tag{6.4c}$$

on the tangential derivatives of φ at C. Although θ, α are continuous at C provided the same coordinates are used throughout the array, the swirl values $\kappa^{\pm}$ are in general not. Thus the approach of Section 4 does not apply in that case.

A set of solutions for circular nozzles with swirl extending that of the zero-swirl case (5.4) is presented in Figure 8. This shows in 8(a), for zero swirl with constant A_n, the same trend throughout cases (i)–(iii) and the same broad range of induced velocities V, although (ii) gives rather different cross-flows and (i) and (iii) are antisymmetric about their middle nozzles. In 8(b) where swirl dominates and V_m is zero in effect there is the same kind of range of W with (iii) being all "on" but $\kappa_n = (-1)^{(n+1)}$ and in essence the neighbours dominate, yielding a regular effect. The vertical range $|W|$ is smaller here and less variation occurs from jet to jet. The antisymmetry about the 11th nozzle is as expected. In 8(c) for a double bank of nozzles the missing W is virtually identical with that labelled "3". The behaviour is much more regular and bounded, and we see an alternating series effect. Also we can reduce the edge effects $|A_n|$ simply by increasing epsilon keeping $|u_0|$ fixed, and increase κ_n by increasing the swirling, i.e. the K values. Further the induced V is as if divergent whereas W is convergent.

https://doi.org/10.1017/S0956792514000448 Published online by Cambridge University Press

6.3 Unsteadiness

With unsteadiness present, the time scale $O(1/L)$ is indicated by the scales in Section 2, say $t = T/L$, and terms $\partial U_1/\partial T, \partial V_1/\partial T, \partial W_1/\partial T$ then need adding on the left in equations (2.5b)–(2.5d) respectively and $\partial\zeta/\partial T$ in equation (2.6a). The contributions $-\partial\zeta_0/\partial T, -\partial U_0/\partial T$ are added to the right-hand sides of equations (2.6a) and (2.6d). Concerning the plug-type setting in Section 4, the so-named constants in equation (4.1a) become functions of T (only) while in equation (4.1b) we have $U_{00}(N, T)$ now. Just before equations (4.2a) and (4.2b) U_1 is $-(dU_0/dT)/U_0$, which however does not affect the subsequent results. Moreover the conditions in equations (4.4c) and (4.4d) remain valid at leading order due to the thinness of the edge layers and the associated large spatial derivatives, except if fast dynamics in the edge layers is particularly pronounced (which would for example add a term $-\partial U_{00}/\partial T$ on the right in (4.5b)). Given that, the substantial unsteady effects are confined to J in equations (4.4c) and (4.4d) becoming time-dependent, $J(T)$, together with the piecewise axial velocities $U_0{}^{\pm}(T)$ acting then on the left of (4.4c).

7 Final comments

It is perhaps apt to start here by considering aspects of the interference between jets and in particular the implications for misdirection of a jet. The general case of Sections 2 and 3 shows up clearly the issue of jet misdirection raised in the introduction. The general case with its smooth axial velocity U_0 and cross-plane vorticity ζ_0 as in Section 2 has controlling equations that illustrate the elliptic nature of the fluid motion in the cross-plane and hence the interdependency of all the jets that are firing at any instant, accentuated by a slow decay with distance in the cross-plane, while in addition the cross-flow velocities are prime indicators of misdirection of any jet since the axial velocity is the largest and is only affected slightly by interaction over the length scales of current industrial concern. We refer to the scalings in Section 2. The findings are supported further by the proof presented in Section 6 of non-periodicity of the jet flow in the general case and are confirmed specifically by the results in Sections 4–6 on interference between rectangular jets, circular jets and comparisons between them. Misdirection seems a common finding although there is some sensitivity to the interference as, for example, neighbouring jets may reverse the cross-flows arising in each other and increased sizes of array can increase it, and we should reiterate the point that the major flow velocity is that in the axial direction so that any misdirection is rather limited. Throughout this the predictions of interaction and misdirection of jets revolve around a phenomenon that is dependent on a number of parameters, on the detailed shapes of nozzles and on the detailed velocity profiles within the jets, unless high precision is unimportant and more qualitative information or guidance is acceptable.

Given that the velocity profiles in the jets emerging from the nozzles play a significant part the present study has been divided into consideration of smooth profiles as the most general case and plug-type profiles as special cases which are close to those of the industrial setting. The latter provide some of the more qualitative information mentioned above. Sample results are presented and described in Sections 4 and 5 for various velocity

https://doi.org/10.1017/S0956792514000448 Published online by Cambridge University Press

ratios and edge effects from the local velocity deficits and many more could be investigated readily. The array flow analysis also works with axial velocity U_0 being zero or close to zero in part of the array of nozzles as a limiting process then applies to the edge conditions in equations (4.4c) and (4.4d). Enhanced cross-flows are observed in the results. The wider interest however remains probably in nonzero axial velocities since the quiescent scenario is an unlikely one during the operation of a sorting machine for example. It is further noteworthy that in the present 3D flow scenario there are effects from two main sources of input, namely the axial velocity U_0 and the cross-plane vorticity ζ_0, and that much of the current analysis has been concentrated on negligible such vorticity as a first central case.

Unsteady effects also deserve more comment. Unsteady influences are discussed in brief in Section 6 mostly in the context of plug flows and at some more length in [11] by means of a model description and examples based on a quasi-steady assumption. The model could be improved upon by using both the viscous contribution U_{0yy} and the scaled acceleration term U_{0T} in the edge layer equations (4.5a) and (4.5b) or adding the contribution U_{0T} and so on to equation (4.4d) but in fact the latter contribution is small compared with U_{0yy} or more generally U_{0nn} because of the scaling inherent in the presence of the thin edge layer. So the acceleration effect seems more likely to appear in the bulks of the jets. It is significant also that we can keep the account here quite short because quasi-steady behaviour dominates in theory and is also believed to hold in the industrial context. The unsteady flow analysis has still to address in full the progress of jet fronts in the current setting and the typical impact of a jet upon a grain but a start has been made in [11].

Miscellaneous points to note in passing here are the following. Laminar flow is considered primarily in the present analysis although the work also applies to the turbulent regime. The latter has turbulent stresses replacing the laminar forms in Sections 2–6 and leads to a much increased viscous thickness and likely shortened development length but otherwise the same basic concept as here. Plug flows are especially appropriate in the turbulent regime. More specifically in the laminar regime the typical scales associated with swirl flow in the cross-plane are relatively small, which in a sense shows the practical benefit of using predominantly axial jets. The scales and structure here are emphasised in Sections 1 and 2. (In response to a referee′s comment we repeat that the correction effects in the asymptotic analysis are of order $1/L$ and L/Re as discussed near the start of Section 2.) Non-superposition of solutions in the plug cases for most circumstances (Section 5.1) is worth mentioning again and can be verified by a perturbation about the equi-velocity examples of Section 5.2. Likewise the potential function ϕ is non-constant in general. Examination of large values of the parameter κ in Section 6 for instance would seem worthwhile. Preliminary investigations of rectangles with swirl have been done. Conformal mapping and other techniques of complex variable theory [18–20] can be applied to Sections 4–6 but the specific examples shown seem to convey the major findings.

Connections with industry can now be reconsidered. Particular issues which need to be addressed concern the angles involved in misdirection and the uniformity of such misdirection. The typical angles can be estimated from the scale analysis presented near the start of the working as being of order $1/L$ and hence approximately 0.013–0.033 or

https://doi.org/10.1017/S0956792514000448 Published online by Cambridge University Press

1–2 degrees say. Broadly the same estimate results from consideration of the velocity components. Hence over the representative axial distance of 150 mm mentioned in the introduction the cross-plane distance is of the order 2–5 mms, in keeping with the nozzle dimensions. This means that for a grain of typical dimension 2–4 mms a distance around 4 mms or so on either side of the grain is also affected significantly by the air jet. Therefore an estimated 4–6 other grains are predicted to be hit collaterally, subject to variations due to averaging of course. The velocity ratio in the nozzle jet and the influence of turbulence [3, 4] would both tend to increase the prediction. As regards the uniformity of misdirection our comments in a preceding paragraph indicate the sensitivity of the interactions between jets and hence the likely variation in misdirection from firing to firing. Yet the typical angles produced can be expected to remain as above and hence on an order of magnitude basis a uniform estimate for the misdirection as used in the 150 mm calculation above seems plausible. Along with this the jump condition in equation (4.4c) for the most realistic case of plug jets involves the velocity ratios v/u essentially and hence angles operating in the X-n plane estimated as before, yielding a net inflow into any edge layer and confirming the jet interactions are bound to misdirect. By contrast, while the long-scale analysis begun in Section 2 shows there is significant cross-flow and the periodic analysis in Section 6 shows cross-flows do not cancel out (in a sense), the working suggests there is potential advantage to moving the target grain nearer the nozzle because of the reduced departure from the centre-line trajectory there, an effect which is linear in axial distance. This may be abetted by several factors: increasing the jet speed or Reynolds number by even a comparatively small amount subject to flow transition; using jets in combination (cf. the Kármán vortex street); swirling the jets especially in an alternating pattern (which reduces the interference significantly); possibly ensuring non-quiescent fluid (given the increased cross-plane activity found when U_0 is small); and possibly pulsing them to some extent although firm evidence for this last is lacking as yet. To repeat, since detailed nozzle-array problems throughout are multi-parameter multi-shape multi-profile ones more qualitative information or guidance as above is likely to be potentially more useful for design requirements. General shapes of nozzle have been accommodated here in principle, bearing in mind that rectangular and circular shapes are the most commonly used in practice at least up to the present time and they produce broadly similar effects. Several possible means to improve design are inherent above and may be relatively easy to implement. The modelling work so far sets out a possibly promising approach although there is clearly much still to do and specific design questions remain from application to application.

Acknowledgements

We thank colleagues Susan Brown, Sergei Timoshin for helpful comments early on, personnel at Buhler-Sortex Ltd. (Sarah Bee, Mark Honeywood, John Low) for their continued interest and questions, as well as EPSRC-CASE, Buhler-Sortex Ltd. and the KTN in Industrial Mathematics concerning funding for PEW. Comments by a referee are also acknowledged.

References

[1] Ellis, A. S. & Smith, F. T. (2008) A continuum model for a chute flow of grains. *SIAM J. Appl. Math.* **69**(2), 305–329.

[2] Ellis, A. S. & Smith, F. T. (2010) On the evolving flow of grains down a chute. *J. Eng. Math.* **68**, 233–247.

[3] Wilson, P. L. & Smith, F. T. (2005) A three-dimensional pipe flow adjusts smoothly to the sudden onset of a bend. *Phys. Fluids* **17**(4), 048102, 1–4.

[4] Wilson, P. L. & Smith, F. T. (2007) The development of the turbulent flow in a bent pipe. *J. Fluid Mech.* **578**, 467–494.

[5] Badra, J., Masri, A. R. & Behnia, M. (2013) Enhanced transient heat transfer from arrays of jets impinging on a moving plate. *Heat Transfer. Eng.* **34**(4), 361–371.

[6] Browne, E. A., Michna, G. J., Jensen, M. K. & Peles, Y. (2010) Microjet array single-phase and flow boiling heat transfer with R134a. *Int. J. Heat Mass Transfer* **53**, 5027–5034.

[7] Scholz, P., Casper, M., Ortmanns, J., Kähler, C. J. & Radespiel, R. (2008) Leading-edge separation control by means of pulsed vortex generator jets. *AIAA J.* **46**(4), 837–846.

[8] Kuibin, P. A., Shtork, S. I. & Fernandes, E. C. (2007) Vortex structure and pressure pulsations in a swirling jet flow. In: *Proc. 5th IASME /WSEAS Int. Conf. Fluid Mech Aerod*, 25–27 August 2007, Athens, Greece.

[9] Maidi , M. & Yao, Y. (2007) On the flow interactions of multiple jets in cross-flow. In: *Proc. 5th IASME /WSEAS Int. Conf. Fluid Mech Aerod*, 25–27 August 2007, Athens, Greece.

[10] Bhat, T. R. S., Baty, R. S. & Morris, P. J. (1990) A linear shock cell model for non-circular jets using a conformal mapping with a pseudo-spectral hybrid scheme. *AIAA* paper no. 90-3960, 13th Aeroacoustics Conference, October 1990.

[11] Westwood, P. E. (2005) Food-sorting jet arrays and target impact properties. *Ph.D. Thesis*, UCL, London.

[12] Smith, F. T. (2002) Interference and turning of in-parallel wakes. *Quart. J. Mech. Appl. Math.* **55**(1), 49–67.

[13] Frigaard, I. A. (1995) The dynamics of spray-formed billets. *SIAM J. Appl. Math.* **55**(5), 1161–1203.

[14] Lu, K. & Shaw, L. (2009) Spray deposition and coating processes. In: *Materials Processing Handbook*, CRC Press, pp. 11-1–11-31, Boca Raton, Florida, USA.

[15] Tadjfar, M. & Smith, F. T. (2004) Direct simulations and modelling of basic three-dimensional bifurcating tube flows. *J. Fluid Mech.* **519**, 1–32.

[16] Bowles,, R. I., Ovenden, N. C. & Smith, F. T. (2008) Multi-branching three-dimensional flow with substantial changes in vessel shapes. *J. Fluid Mech.* **614**, 329–354.

[17] Smith,, F. T., Purvis, R., Dennis, S. C. R., Jones, M. A., Ovenden, N. C. & Tadjfar, M. (2003) Fluid Flow through various branching tubes. *J. Eng. Math.* **47**, 277–298.

[18] Milne-Thomson, L. M. (1968) *Theoretical Hydrodynamics*, 5th ed., Macmillan and Co Ltd., London.

[19] Carrier, G. F., Krook, M. & Pearson, C. E. (1966) *Functions of a Complex Variable: Theory and Technique*, McGraw Hill, New York.

[20] Kirchhoff, R. H. Inviscid incompressible flow - potential flow. In: R.W. Johnson (editor), *Handbook of Fluid Dynamics*, Ch 7, CRC Press, Boca Raton, Florida, USA.